 CMC, vol.1, no.1, pp.91-105, 2004

Elasto-plastic Analysis of Two-dimensional Orthotropic Bodies with the Boundary Element Method

X.S. Sun[1], L.X. Huang[1], Y.H. Liu[1] and Z.Z. Cen[1,2]

Abstract: The Boundary Element Method (BEM) is introduced to analyze the elasto-plastic problems of 2-D orthotropic bodies. With the help of known boundary integral equations and fundamental solutions, a numerical scheme for elasto-plastic analysis of 2-D orthotropic problems with the BEM is developed. The Hill orthotropic yield criterion is adopted in the plastic analysis. The initial stress method and tangent predictor-radial return algorithm are used to determine the stress state in solving the nonlinear equation with the incremental iteration method. Finally, numerical examples show that the BEM is effective and reliable in analyzing elasto-plastic problems of orthotropic bodies.

keyword: Boundary Element Method (BEM), Elasto-plastic Analysis, Singular Integrals, 2-D Orthotropic Body, Orthotropic Yield Criterion

1 Introduction

Nowadays new type materials exhibiting a characteristic of anisotropy or orthotropy are widely used in the industries and the corresponding numerical analysis is necessary to solve these complicated problems as the experiments are absent or the analytical methods are unfeasible in most conditions. Elasto-plastic analysis is one of the practical and desirable problems, which has attracted many interests on study. However, the anisotropic or orthotropic plastic analysis is much more complicated than isotropic problems. Fortunately, the development of computer technologies and computational methods permits a more realistic and complex modeling than ever before. The finite element method (FEM) and the boundary element method (BEM) are two usual numerical methods that are widely used in solving many engineering problems. In general, the FEM is more mature and popular, and many elasto-plastic analysis on orthotropic problems have been implemented with the FEM in the past (Owen and Figuerias, 1983; Vaziri, Olson and Anderson, 1992; Karakuzu and Sayman, 1994). But the BEM is more effective and professional in some problems such as stress concentration, and it has been successfully exploited to solve many kinds of isotropic problems, including elastic, thermo-elastic, elasto-plastic, dynamic, contact, fracture and coupling problems, etc. (Brebbia, Telles and Wrobel, 1984; Du et al, 1989; Aliabadi, 2002) It should also be pointed out that in certain elasto-plastic problems the BEM can prove to be very efficient. For example, better accuracy can be obtained only with less discretized meshes in the BEM than that in the FEM; on the other hand, if the plastic zone is limited compared with the domain of the considered body, the BEM allows discretization of only this limited plastic region, rather than that of the entire domain as is needed for the FEM, which is much more effective when the plastic zone appears in the field around the boundary in some cases such as stress concentration or contact problems.

The BEM was first introduced to analyze elasto-plastic problems for 3-D isotropic bodies by Swedlow and Cruse (1971). Mendelson (1973) later improved Swedlow and Cruse's work and gave the expressions for internal stress and strain for both 2-D and 3-D isotropic problems. Mukherjee (1977), Kumar and Mukherjee (1977) and Bui (1978) corrected successively some errors in the previous works. Telles and Brebbia (1979) presented the complete BEM formulations for 2-D and 3-D elasto-plastic problems of isotropic materials based on the initial strain method. Banerjee, Cathie and Davies (1979) established the boundary integral equations for 2-D and 3-D elasto-plastic problems based on the initial stress method. Cen (1984) developed the BEM in coupling with the FEM to solve efficiently 3-D elasto-plastic problems.

[1] (Dept. of Engineering Mechanics, Tsinghua University, Beijing 100084, P. R. China)
[2] Corresponding author.
Tel: +86-10-62784015; fax: +86-10-62770349
Email address: demczz@tsinghua.edu.cn (Z.Z. Cen)

Since then the BEM on elasto-plastic analysis has been developed mainly on two aspects: one is the alternative solutions for removing domain discretization (Henry and Banerjee, 1988; Partridge, Brebbia and Wrobel, 1992; Ochiai and Kobayashi, 1999) or for removing strong singularities in the integral equations (Okada, Rajiyah and Atluri, 1989; Okada and Atluri, 1994); and the other is the solution strategies for solving the nonlinear system equations (Banerjee, Henry and Raveendra, 1989; Chopra and Dargush, 1994; Bonnet and Mukherjee, 1996). Moreover, the BEM also appeared to solve other problems related to elasto-plasticity, such as dynamics elasto-plastic problems (Carrer and Telles, 1992), elasto-plastic contact problems (Dong, 1992) and thermal elasto-plastic problems (Sladek and Sladek, 1995). It should be noted that all the above elasto-plastic studies with the BEM only deal with the problems for isotropic materials. However, up to now, the application of the BEM to elasto-plastic analysis of orthotropic or anisotropic problems has not been completely solved. Therefore, further discussions on the application of the BEM are necessary, especially about the elasto-plastic analysis of orthotropic bodies.

As to the application of the BEM to orthotropic or anisotropic problems, some studies were mainly focused on elastic problems so far. Green (1943) first introduced the fundamental solutions for 2-D orthotropic bodies under a concentrated force. Rizzo and Shippy (1970) introduced the fundamental solutions into the boundary integral equations for numerical elastic analysis of stress concentration. Recently, Sun and Cen (2002) improved and extended these fundamental solutions into elasto-plastic problems and established the boundary integral equations for elasto-plastic analysis of 2-D orthotropic bodies, but neither numerical techniques nor results were described. Huang et al (2004) used these improved fundamental solutions to implement parameter identification for 2-D orthotropic plates with the BEM. Besides these above studies, Tan and Gao (1992) analyzed the stress concentrations and cracks of plane anisotropic bodies and analytical expressions for the stress intensity factors were derived in terms of the tractions or displacements. Dong, Lo and Cheung (1992) also exploited the BEM to analyze elastic inclusion problems for orthotropic and anisotropic materials. Zhang (2002) presented a 2-D time-domain boundary integral equation method for transient dynamic analysis of cracked orthotropic solids. However, to our knowledge, elasto-plastic analysis of orthotropic bodies with the BEM has not been studied so far.

This paper will introduce the application of the BEM to 2-D elasto-plastic problems for orthotropic bodies. The discretized equations and iterative equations for numerical implementation are presented based on the boundary integral equations, internal values and fundamental solutions for orthotropic bodies (Sun and Cen, 2002), and the elasto-plastic analysis of 2-D orthotropic problems is discussed. The Hill orthotropic yield criterion is adopted in the plastic analysis. The initial stress method and tangent predictor-radial return algorithm are used to determine the stress state in solving the nonlinear equation with the incremental iteration method. Two numerical examples will be presented to demonstrate the validity and reliability of the proposed numerical scheme. The computational results will also be compared to the existing ones or those obtained from the FEM using the commercial code ABAQUS.

2 Basic Equations

2.1 Linear elastic orthotropic constitutive equation

For convenience, the following discussion is based on the rectangular Cartesian coordinate system and the vector or matrix denotation is adopted for the major variables. For the case of plane stress, according to the generalized linear Hooke's law, the elastic orthotropic constitutive relations of stress and strain can be written with matrix as (Lekhnitskii, 1968):

$$\boldsymbol{\sigma} = \mathbf{D}\boldsymbol{\varepsilon} \ \ (\text{or } \boldsymbol{\varepsilon} = \mathbf{S}\boldsymbol{\sigma}) \tag{1}$$

where $\mathbf{D} = \mathbf{S}^{-1}$ is the 3×3 elastic constant matrix and $\mathbf{S}$ can be written with the compliances or engineering constants as:

$$\begin{aligned} \mathbf{S} &= \begin{bmatrix} S_{11} & S_{12} & 0 \\ S_{21} & S_{22} & 0 \\ 0 & 0 & S_{66} \end{bmatrix} \\ &= \begin{bmatrix} 1/E_1 & -\nu_{12}/E_1 & 0 \\ -\nu_{12}/E_1 & 1/E_2 & 0 \\ 0 & 0 & 1/G_{12} \end{bmatrix} \end{aligned} \tag{2}$$

where E_1, E_2 are the Young's moduli in the two in-plane principal material directions, respectively; G_{12} is the in-plane shear modulus; ν_{12} is the Poisson's ratio and conforms to the relation $\nu_{12}/E_1 = \nu_{21}/E_2$.

The stress and strain in Eq.(1) take respectively the vector form as follows:

$$\boldsymbol{\sigma} = \left[\begin{array}{ccc} \sigma_1 & \sigma_2 & \tau_{12} \end{array} \right]^{\mathrm{T}} \tag{3}$$

$$\boldsymbol{\varepsilon} = \left[\begin{array}{ccc} \varepsilon_1 & \varepsilon_2 & \gamma_{12} \end{array} \right]^{\mathrm{T}} \tag{4}$$

where superscript T denotes the transpose of a vector or matrix.

2.2 Orthotropic yield criterion

For an orthotropic material, Hill (1948) first introduced a yield function expressed by yield strengths in the principal material directions and shear strengths in planes, i.e. Hill orthotropic yield criterion. This criterion is also an extension of the von Mises criterion for isotropic materials, and it is used widely in many plastic problems and creep problems in which reasonable results are demonstrated. In the case of plane stress, Hill yield criterion can be written as:

$$\frac{\sigma_1^2}{X^2} - \frac{\sigma_1\sigma_2}{X^2} + \frac{\sigma_2^2}{Y^2} + \frac{\tau_{12}^2}{S^2} = 1 \tag{5}$$

where X, Y are the strength properties in principal material direction 1 and 2 respectively; S is the shear strength property in plane. If $X = Y = \sqrt{3}S = \sigma_Y$, Eq.(5) is reduced to von Mises criterion for isotropic materials.

If the equivalent yielding strength $\overline{\sigma}_0$ is defined as:

$$\overline{\sigma}_0 = X \tag{6}$$

then Hill orthotropic yield criterion can also be rewritten in the following function form:

$$f(\boldsymbol{\sigma}) = \frac{1}{3}\boldsymbol{\sigma}^{\mathrm{T}}\mathbf{H}\boldsymbol{\sigma} - \frac{1}{3}\overline{\sigma}_0^2 = 0 \tag{7}$$

where $\mathbf{H}$ is the Hill orthotropic coefficient matrix and

$$\mathbf{H} = \begin{bmatrix} 1 & -1/2 & 0 \\ -1/2 & H_1 & 0 \\ 0 & 0 & H_2 \end{bmatrix} \tag{8}$$

$$H_1 = \frac{X^2}{Y^2},\ H_2 = \frac{X^2}{S^2} \tag{9}$$

and the equivalent stress $\overline{\sigma} = \sqrt{\boldsymbol{\sigma}^{\mathrm{T}}\mathbf{H}\boldsymbol{\sigma}}$ can also be defined.

It is obvious that $H_1 = 1,\ H_2 = 3$ for von Mises criterion.

2.3 Plastic flow rule

In the elasto-plastic analysis with infinitesimal deformation, the strain $\dot{\boldsymbol{\varepsilon}}$, marked by rate (or increment), can be divided into two parts, i.e. elastic and plastic part respectively:

$$\dot{\boldsymbol{\varepsilon}} = \dot{\boldsymbol{\varepsilon}}^e + \dot{\boldsymbol{\varepsilon}}^p \tag{10}$$

The plastic flow rule, which determines the direction of plastic straining, can be expressed through the normal of plastic strain increment and the yield surface as (Hill, 1983):

$$\dot{\boldsymbol{\varepsilon}}^p = \dot{\lambda}\frac{\partial f}{\partial \boldsymbol{\sigma}} = \dot{\lambda}\mathbf{a} \tag{11}$$

where $\dot{\lambda}$ is the plastic multiplier that determines the amount of plastic strain and $\mathbf{a}$ is termed as the flow vector. If the yield function $f(\boldsymbol{\sigma})$ takes the form of Eq.(7), vector $\mathbf{a}$ can be written as:

$$\mathbf{a} = \frac{\partial f}{\partial \boldsymbol{\sigma}} = \frac{2}{3}\mathbf{H}\boldsymbol{\sigma} \tag{12}$$

For an orthotropic material with ideal plasticity, the plastic multiplier $\dot{\lambda}$ can be obtained through the consistency conditions as:

$$\dot{\lambda} = \frac{\mathbf{a}^{\mathrm{T}}\mathbf{D}\dot{\boldsymbol{\varepsilon}}}{\gamma_0} \tag{13}$$

where

$$\gamma_0 = \mathbf{a}^{\mathrm{T}}\mathbf{D}\mathbf{a} \tag{14}$$

2.4 Elasto-plastic orthotropic constitutive equation

For infinitesimal deformation, if the initial plastic stress (or plastic strain) is considered, according to Hooke's law, the relation of stress rate and strain rate including plastic stress (or plastic strain), i.e. the constitutive equation, can be written with matrix as:

$$\dot{\boldsymbol{\sigma}} = \mathbf{D}\dot{\boldsymbol{\varepsilon}} - \dot{\boldsymbol{\sigma}}^p \ (\text{or } \dot{\boldsymbol{\varepsilon}} = \mathbf{S}\dot{\boldsymbol{\sigma}}^e + \dot{\boldsymbol{\varepsilon}}^p) \tag{15}$$

where $\dot{\boldsymbol{\sigma}}^e$, $\dot{\boldsymbol{\sigma}}^p$ are virtual elastic stress rate and plastic stress rate, respectively. All these stress or strain variables take the similar vector form as that in Eq.(3) and Eq.(4), and

$$\dot{\boldsymbol{\sigma}} = \dot{\boldsymbol{\sigma}}^e - \dot{\boldsymbol{\sigma}}^p \tag{16}$$

$$\dot{\boldsymbol{\sigma}}^p = \mathbf{D}\dot{\boldsymbol{\varepsilon}}^p (\text{or } \dot{\boldsymbol{\varepsilon}}^p = \mathbf{S}\dot{\boldsymbol{\sigma}}^p) \tag{17}$$

With the help of Eqs.(11), (13), (14), (16) and (17), the elasto-plastic relation of stress and strain with ideal plasticity can be expressed by rate as:

$$\dot{\boldsymbol{\sigma}} = \dot{\boldsymbol{\sigma}}^e - \frac{\mathbf{D}\mathbf{a}\mathbf{a}^{\mathrm{T}}\mathbf{D}}{\mathbf{a}^{\mathrm{T}}\mathbf{D}\mathbf{a}}\dot{\boldsymbol{\varepsilon}} \tag{18}$$

3 Boundary Element Implementation

3.1 Boundary integral equation and fundamental solutions

The boundary integral equation for 2-D orthotropic elasto-plastic problems and corresponding internal virtual elastic stress integral equations have been given as (Sun and Cen, 2002):

$$\mathbf{c}\dot{\mathbf{u}} = \int_\Gamma \mathbf{u}^*\dot{\mathbf{t}}\mathrm{d}\Gamma - \int_\Gamma \mathbf{t}^*\dot{\mathbf{u}}\mathrm{d}\Gamma + \int_\Omega \mathbf{u}^*\dot{\mathbf{f}}\mathrm{d}\Omega + \int_\Omega \boldsymbol{\sigma}^*\dot{\boldsymbol{\varepsilon}}^p\mathrm{d}\Omega \tag{19a}$$

$$\dot{\boldsymbol{\sigma}}^e = \int_\Gamma (-\boldsymbol{\sigma}^*)^{\mathrm{T}}\dot{\mathbf{t}}\mathrm{d}\Gamma - \int_\Gamma \mathbf{t}_p^*\dot{\mathbf{u}}\mathrm{d}\Gamma + \int_\Omega (-\boldsymbol{\sigma}^*)^{\mathrm{T}}\dot{\mathbf{f}}\mathrm{d}\Omega + \int_\Omega \boldsymbol{\sigma}_p^*\dot{\boldsymbol{\varepsilon}}^p\mathrm{d}\Omega + \dot{\boldsymbol{\sigma}}^{eV} \tag{20a}$$

where the variables with the superscript asterisk "*" denote the fundamental solutions (matrix form) in the BEM; matrix **c** is termed the boundary properties and $\dot{\boldsymbol{\sigma}}^{eV}$ denotes the free term for strong singularity in domain which can be expressed as:

$$\dot{\boldsymbol{\sigma}}^{eV} = \left(\mathbf{E}^V + \mathbf{D}\right)\dot{\boldsymbol{\varepsilon}}^p = \left(\mathbf{E}^V\mathbf{S} + \mathbf{I}\right)\dot{\boldsymbol{\sigma}}^p \tag{21}$$

The further details can be found in the paper of Sun and Cen (2002). The plastic stress is considered here as the initial stress. As the following equation holds true:

$$\int_\Omega \boldsymbol{\sigma}_p^*\dot{\boldsymbol{\varepsilon}}^p\mathrm{d}\Omega = \int_\Omega \boldsymbol{\sigma}_p^*(\mathbf{S}\dot{\boldsymbol{\sigma}}^p)\,\mathrm{d}\Omega = \int_\Omega \left(\boldsymbol{\sigma}_p^*\mathbf{S}\right)\dot{\boldsymbol{\sigma}}^p\mathrm{d}\Omega = \int_\Omega \boldsymbol{\varepsilon}_p^*\dot{\boldsymbol{\sigma}}^p\mathrm{d}\Omega \tag{22}$$

then Eq.(19a) and Eq.(20a) can be written alternatively with initial plastic stress as:

$$\mathbf{c}\dot{\mathbf{u}} = \int_\Gamma \mathbf{u}^*\dot{\mathbf{t}}\mathrm{d}\Gamma - \int_\Gamma \mathbf{t}^*\dot{\mathbf{u}}\mathrm{d}\Gamma + \int_\Omega \mathbf{u}^*\dot{\mathbf{f}}\mathrm{d}\Omega + \int_\Omega \boldsymbol{\varepsilon}^*\dot{\boldsymbol{\sigma}}^p\mathrm{d}\Omega \tag{19b}$$

$$\dot{\boldsymbol{\sigma}}^e = \int_\Gamma (-\boldsymbol{\sigma}^*)^{\mathrm{T}}\dot{\mathbf{t}}\mathrm{d}\Gamma - \int_\Gamma \mathbf{t}_p^*\dot{\mathbf{u}}\mathrm{d}\Gamma + \int_\Omega (-\boldsymbol{\sigma}^*)^{\mathrm{T}}\dot{\mathbf{f}}\mathrm{d}\Omega + \int_\Omega \boldsymbol{\varepsilon}_p^*\dot{\boldsymbol{\sigma}}^p\mathrm{d}\Omega + \dot{\boldsymbol{\sigma}}^{eV} \tag{20b}$$

and the displacements at internal points can also be given as:

$$\dot{\mathbf{u}} = \int_\Gamma \mathbf{u}^*\dot{\mathbf{t}}\mathrm{d}\Gamma - \int_\Gamma \mathbf{t}^*\dot{\mathbf{u}}\mathrm{d}\Gamma + \int_\Omega \mathbf{u}^*\dot{\mathbf{f}}\mathrm{d}\Omega + \int_\Omega \boldsymbol{\varepsilon}^*\dot{\boldsymbol{\sigma}}^p\mathrm{d}\Omega \tag{23}$$

All the fundamental solutions in the above equations take the following matrix forms:

$$\mathbf{u}^* = \begin{bmatrix} u_{11}^* & u_{12}^* \\ u_{21}^* & u_{22}^* \end{bmatrix}, \quad \mathbf{t}^* = \begin{bmatrix} t_{11}^* & t_{12}^* \\ t_{21}^* & t_{22}^* \end{bmatrix} \tag{24}$$

$$\boldsymbol{\varepsilon}^* = \begin{bmatrix} \varepsilon_{111}^* & \varepsilon_{122}^* & \gamma_{112}^* \\ \varepsilon_{211}^* & \varepsilon_{222}^* & \gamma_{212}^* \end{bmatrix}, \quad \boldsymbol{\sigma}^* = \begin{bmatrix} \sigma_{111}^* & \sigma_{122}^* & \sigma_{112}^* \\ \sigma_{211}^* & \sigma_{222}^* & \sigma_{212}^* \end{bmatrix} \tag{25}$$

$$\boldsymbol{\varepsilon}_p^* = \begin{bmatrix} \varepsilon_{1111}^* & \varepsilon_{1122}^* & \gamma_{1112}^* \\ \varepsilon_{2211}^* & \varepsilon_{2222}^* & \gamma_{2212}^* \\ \varepsilon_{1211}^* & \varepsilon_{1222}^* & \gamma_{1212}^* \end{bmatrix}, \quad \boldsymbol{\sigma}_p^* = \begin{bmatrix} \sigma_{1111}^* & \sigma_{1122}^* & \sigma_{1112}^* \\ \sigma_{2211}^* & \sigma_{2222}^* & \sigma_{2212}^* \\ \sigma_{1211}^* & \sigma_{1222}^* & \sigma_{1212}^* \end{bmatrix} \tag{26}$$

$$\mathbf{t}_p^* = \begin{bmatrix} t_{111}^* & t_{112}^* \\ t_{221}^* & t_{222}^* \\ t_{121}^* & t_{122}^* \end{bmatrix} \tag{27}$$

where $\gamma_{i12} = 2\varepsilon_{i12}$, $\gamma_{ij12} = 2\varepsilon_{ij12}$ $(i, j = 1, 2)$ and the components can be found in the paper of Sun and Cen (2002). Additionally, Eq.(22) suggests that $\boldsymbol{\varepsilon}_p^* = \boldsymbol{\sigma}_p^*\mathbf{S}$ (or $\boldsymbol{\sigma}_p^* = \boldsymbol{\varepsilon}_p^*\mathbf{D}$), so these two fundamental solutions are equivalent and depends on the considered initial stress or initial strain.

3.2 Discretized formulation of integral equations

Assume *n* boundary elements (one-dimensional element) and *m* internal cells (two-dimensional element) are discretized in the boundary and domain, respectively, then

the boundary elements and the internal cells are interpolated with one- and two-dimensional interpolation functions, respectively. For example, the 3-node quadratic interpolation function $\mathbf{N}_b(\xi)$ and 4-node quadrilateral linear interpolation function $\mathbf{N}_p(\xi_1,\xi_2)$ are adopted here for the boundary elements and internal cells, respectively. The displacements and tractions on the boundary elements and the plastic stress rates in the internal cells can be expressed by the following equations, respectively:

$$\begin{cases} \dot{\mathbf{u}} = \mathbf{N}_b \dot{\mathbf{u}}^{el},\ \dot{\mathbf{t}} = \mathbf{N}_b \dot{\mathbf{t}}^{el} \\ \dot{\boldsymbol{\sigma}}^p = \mathbf{N}_p \left(\dot{\boldsymbol{\sigma}}^p\right)^{el} \end{cases} \tag{28}$$

where the superscript "*el*" denotes the nodal values in an boundary element or internal cell. With the absence of body force $\dot{\mathbf{f}}$, substituting the interpolated results in Eq.(28) into Eqs.(19b), (20b) and (23) respectively yields:

$$\begin{aligned} &\mathbf{c}_i \dot{\mathbf{u}}_i \\ &= \sum_{k=1}^{n_1} \left[\left(\int_{\Gamma_k} \mathbf{u}^* \mathbf{N}_b \mathrm{d}\Gamma \right) \dot{\bar{\mathbf{t}}}_k^{el} \right] + \sum_{k=n_1+1}^{n} \left[\left(\int_{\Gamma_k} \mathbf{u}^* \mathbf{N}_b \mathrm{d}\Gamma \right) \dot{\mathbf{t}}_k^{el} \right] \\ &- \sum_{k=n_1+1}^{n} \left[\left(\int_{\Gamma_k} \mathbf{t}^* \mathbf{N}_b \mathrm{d}\Gamma \right) \dot{\bar{\mathbf{u}}}_k^{el} \right] - \sum_{k=1}^{n_1} \left[\left(\int_{\Gamma_k} \mathbf{t}^* \mathbf{N}_b \mathrm{d}\Gamma \right) \dot{\mathbf{u}}_k^{el} \right] \\ &+ \sum_{k=1}^{m} \left[\left(\int_{\Omega_k} \boldsymbol{\varepsilon}^* \mathbf{N}_p \mathrm{d}\Omega \right) \left(\dot{\boldsymbol{\sigma}}^p\right)_k^{el} \right] \end{aligned} \tag{29}$$

$$\begin{aligned} &\dot{\boldsymbol{\sigma}}^e \\ &= \sum_{k=1}^{n_1} \left[\left(\int_{\Gamma_k} \left(-\boldsymbol{\sigma}^*\right)^{\mathrm{T}} \mathbf{N}_b \mathrm{d}\Gamma \right) \dot{\bar{\mathbf{t}}}_k^{el} \right] \\ &+ \sum_{k=n_1+1}^{n} \left[\left(\int_{\Gamma_k} \left(-\boldsymbol{\sigma}^*\right)^{\mathrm{T}} \mathbf{N}_b \mathrm{d}\Gamma \right) \dot{\mathbf{t}}_k^{el} \right] \\ &- \sum_{k=n_1+1}^{n} \left[\left(\int_{\Gamma_k} \mathbf{t}_p^* \mathbf{N}_b \mathrm{d}\Gamma \right) \dot{\bar{\mathbf{u}}}_k^{el} \right] - \sum_{k=1}^{n_1} \left[\left(\int_{\Gamma_k} \mathbf{t}_p^* \mathbf{N}_b \mathrm{d}\Gamma \right) \dot{\mathbf{u}}_k^{el} \right] \\ &+ \sum_{k=1}^{m} \left[\left(\int_{\Omega_k} \boldsymbol{\varepsilon}_p^* \mathbf{N}_p \mathrm{d}\Omega \right) \left(\dot{\boldsymbol{\sigma}}^p\right)_k^{el} \right] + \dot{\boldsymbol{\sigma}}^{eV} \end{aligned} \tag{30}$$

$$\begin{aligned} &\dot{\mathbf{u}} \\ &= \sum_{k=1}^{n_1} \left[\left(\int_{\Gamma_k} \mathbf{u}^* \mathbf{N}_b \mathrm{d}\Gamma \right) \dot{\bar{\mathbf{t}}}_k^{el} \right] + \sum_{k=n_1+1}^{n} \left[\left(\int_{\Gamma_k} \mathbf{u}^* \mathbf{N}_b \mathrm{d}\Gamma \right) \dot{\mathbf{t}}_k^{el} \right] \\ &- \sum_{k=n_1+1}^{n} \left[\left(\int_{\Gamma_k} \mathbf{t}^* \mathbf{N}_b \mathrm{d}\Gamma \right) \dot{\bar{\mathbf{u}}}_k^{el} \right] - \sum_{k=1}^{n_1} \left[\left(\int_{\Gamma_k} \mathbf{t}^* \mathbf{N}_b \mathrm{d}\Gamma \right) \dot{\mathbf{u}}_k^{el} \right] \\ &+ \sum_{k=1}^{m} \left[\left(\int_{\Omega_k} \boldsymbol{\varepsilon}^* \mathbf{N}_p \mathrm{d}\Omega \right) \left(\dot{\boldsymbol{\sigma}}^p\right)_k^{el} \right] \end{aligned} \tag{31}$$

The same implementation is carried throughout all the nodes. The knowns and unknowns in Eqs.(29), (30) and (31) are reordered, and then the following equations can be obtained in assembling matrix:

$$\begin{cases} \mathbf{A}\dot{\mathbf{X}} = \dot{\mathbf{F}} + \mathbf{Q}_x \dot{\boldsymbol{\Sigma}}^p \\ \dot{\boldsymbol{\Sigma}}^e = -\mathbf{A}_s \dot{\mathbf{X}} + \dot{\mathbf{F}}_s + \mathbf{Q}_s \dot{\boldsymbol{\Sigma}}^p \\ \dot{\mathbf{U}} = -\mathbf{A}_u \dot{\mathbf{X}} + \dot{\mathbf{F}}_u + \mathbf{Q}_u \dot{\boldsymbol{\Sigma}}^p \end{cases} \tag{32}$$

where $\dot{\mathbf{X}}$ is the unknown array for boundary values; $\dot{\mathbf{F}}$, $\dot{\mathbf{F}}_s$ and $\dot{\mathbf{F}}_u$ are the known arrays for boundary values; $\dot{\mathbf{U}}$, $\dot{\boldsymbol{\Sigma}}^e$ and $\dot{\boldsymbol{\Sigma}}^p$ denote the arrays of displacements, virtual elastic and plastic stresses respectively which consist of the vectors in all nodes; $\mathbf{A}$, $\mathbf{A}_s$ and $\mathbf{A}_u$ denote the assembling coefficient matrices for unknowns; and $\mathbf{Q}_x$, $\mathbf{Q}_s$ and $\mathbf{Q}_u$ denote the assembling coefficient matrices for plastic stress and $\mathbf{Q}_s = \mathbf{Q}'_s + \mathbf{Q}_V$ in which $\mathbf{Q}_V$ comes from the terms for strong singularity. Solving Eq.(32) yields the following equations:

$$\begin{cases} \dot{\mathbf{X}} = \dot{\mathbf{y}} + \mathbf{R}\dot{\boldsymbol{\Sigma}}^p \\ \dot{\boldsymbol{\Sigma}}^e = \dot{\mathbf{s}} + \mathbf{T}_s \dot{\boldsymbol{\Sigma}}^p \\ \dot{\mathbf{U}} = \dot{\mathbf{w}} + \mathbf{T}_u \dot{\boldsymbol{\Sigma}}^p \end{cases} \tag{33}$$

where $\dot{\mathbf{y}} = \mathbf{A}^{-1}\dot{\mathbf{F}}$, $\dot{\mathbf{s}} = \dot{\mathbf{F}}_s - \mathbf{A}_s\mathbf{A}^{-1}\dot{\mathbf{F}}$ and $\dot{\mathbf{w}} = \dot{\mathbf{F}}_u - \mathbf{A}_u\mathbf{A}^{-1}\dot{\mathbf{F}}$, which denote the elastic solutions; $\mathbf{R} = \mathbf{A}^{-1}\mathbf{Q}_x$, $\mathbf{T}_s = \mathbf{Q}_s - \mathbf{A}_s\mathbf{A}^{-1}\mathbf{Q}_x$, $\mathbf{T}_u = \mathbf{Q}_u - \mathbf{A}_u\mathbf{A}^{-1}\mathbf{Q}_x$, and the last terms on the right-hand side of Eq.(33) denote the extra ones for plastic deformation.

3.3 Numerical integral scheme

Numerical quadrature should be used to compute the integrals in Eqs.(29) $\sim$ (31). The general Gaussian quadrature is adopted here for non-singular integrals, but the singular integrals should be treated specially. The terms resulted in singularity include weak singularities involved $\ln r_i^{-1}$ in the boundary and r_i^{-1} in the domain, strong singularities involved r_i^{-1} in the boundary and r_i^{-2} in the domain , and hypersingularity involved r_i^{-2} in the boundary, where r_i $(i = 1,2)$ is the equivalent distance related to the orthotropic elastic constants.

For the weak singularities in the boundary or domain, i.e. integrals involved $\ln r_i^{-1}$ or r_i^{-1}, the singularities can be removed by transformations. With the interpolation functions and the nodal values in the boundary element, the integrals involved $\ln r_i^{-1}$ in the boundary can be transformed to two parts including a logarithmic integral and

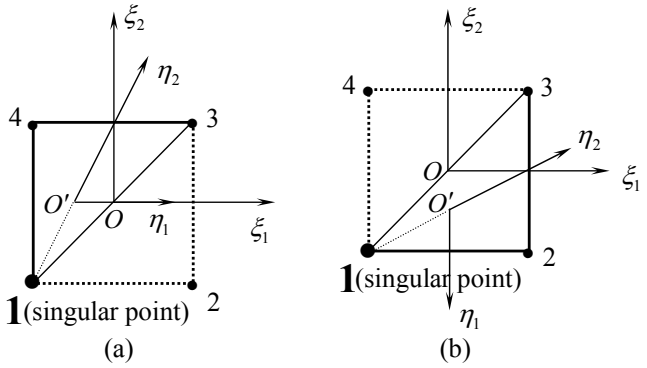

Figure 1 : Internal cell subdivisions (singularity in node 1 is exampled)

a non-singular integral, i.e.

$$\int_\Gamma \ln\frac{1}{r_i}\mathrm{d}\Gamma = \int_0^1 \ln\frac{1}{\eta} J_\xi J_\eta \mathrm{d}\eta + \int_{-1}^1 \ln\frac{1}{\sqrt{\alpha_i f_1^2 + f_2^2}} J_\xi \mathrm{d}\xi \tag{34}$$

then the two terms on the right-hand-side can be calculated by the logarithmic quadrature formula and Gaussian quadrature formula, respectively. The integrals involved r_i^{-1} in the domain can be treated by appropriate coordinate transformation, in which a 4-node quadrilateral cell is divided into two triangles (Fig. 1) and the singular integrals can be calculated with:

$$\int_{\Omega_k} \boldsymbol{\varepsilon}^* \mathbf{N}_p(\xi_1,\xi_2)\mathrm{d}\Omega = \sum_{k=1}^{2}\int_{-1}^{1}\int_{-1}^{1} \boldsymbol{\varepsilon}^* \mathbf{N}_p(\eta_1,\eta_2) J_\xi J_\eta^{(k)} \mathrm{d}\eta_1 \mathrm{d}\eta_2 \tag{35}$$

where

$$J_\eta^{(k)} = \frac{1}{2}(1+\eta_2) = o(r_i),\ (k=1,2) \tag{36}$$

and the original local coordinates system (ξ_1,ξ_2) is transformed into a new one (η_1,η_2). This transformation results in the Jacobian $J_\eta^{(k)},\ (k=1,2)$ proportional to r_i and accordingly the singularity r_i^{-1} is removed.

The strong singularity, involved r_i^{-1} and r_i^{-2} in the boundary and domain respectively, can be removed by indirect methods of rigid displacement solution and constant plastic strain solution, respectively. The rigid displacement solution of Eq.(29), where $\dot{\mathbf{u}}_0 = I$ (2×2 unit matrix) and , can result in the following equation:

$$\mathbf{c}_i + \int_{\Gamma_i} \mathbf{t}^* \mathbf{N}_b \mathrm{d}\Gamma = -\sum_{\substack{j=1 \\ i\neq j}}^{n} \left(\int_{\Gamma_j} \mathbf{t}^* \mathbf{N}_b \mathrm{d}\Gamma \right) \tag{37}$$

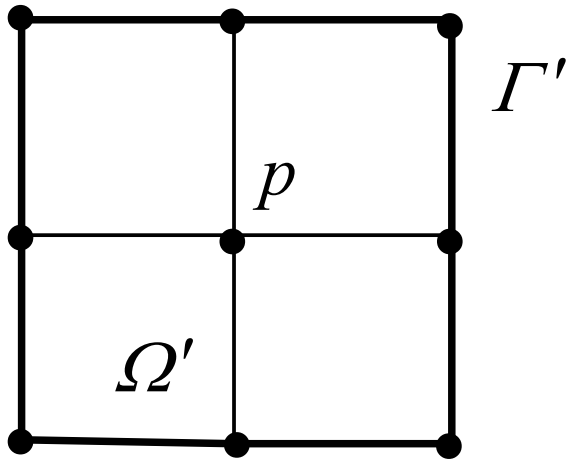

Figure 2 : Cells connected to an internal singular point p

Then the boundary singular integrals involved r_i^{-1} are calculated indirectly by summation of the non-singular integrals with Eq.(37). For an internal singular point p, four cells are connected around, which composes a sub-domain Ω' with sub-boundary Γ' including eight one-dimensional linear elements (Fig. 2). If all the nodes at the singular point p for four cells are locally numbered "1", the constant plastic strain solution of Eq.(30), where $\dot{\boldsymbol{\varepsilon}}_0^p = I$ (3×3 unit matrix) and $\dot{\boldsymbol{\sigma}} = 0,\ \dot{\mathbf{t}} = 0$, will result in this equation in sub-domain Ω':

$$\sum_{k=1}^{4}\int_{\Omega_k'} \boldsymbol{\varepsilon}_p^* \mathbf{N}_p^{(1)} \mathrm{d}\Omega + \mathbf{E}^V \mathbf{S} = \sum_{k=1}^{8}\int_{\Gamma_k'} \mathbf{t}_p^* \dot{\mathbf{U}}_0 \mathrm{d}\Gamma - \sum_{k=1}^{4}\sum_{i=2}^{4}\int_{\Omega_k'} \boldsymbol{\varepsilon}_p^* \mathbf{N}_p^{(i)} \mathrm{d}\Omega \tag{38}$$

where $\dot{\mathbf{U}}_0$ is the displacement solution under the constant plastic strain and takes the following matrix:

$$\dot{\mathbf{U}}_0 = \begin{bmatrix} S_{11}x_1 & S_{12}x_1 & \frac{1}{2}S_{66}x_2 \\ S_{12}x_2 & S_{22}x_2 & \frac{1}{2}S_{66}x_1 \end{bmatrix}_{(2\times 3)} \tag{39}$$

where $x_i = x_i^q - x_i^p$ $(i = 1,2)$ is the distance between the field point q and source point p. Then similar to Eq.(37), the domain singular integrals involved $r_{,i}^{-2}$ are calculated indirectly by summation of the non-singular integrals and known sub-boundary integrals.

The hypersingularity involved $r_{,i}^{-2}$ in the boundary only appears when the boundary stress is considered with the internal stress integral equations. In some previous works, a weighted residual method was used to derive the integral equations (BIE), and a formulation of weak-singular BIE, which doesn't involve the hyper-singularity any more, was established to solve finite/small strain elastoplastic problems (Okada and Atluri, 1994; Han and Atluri, 2003; Atluri, Han and Shen, 2003). Additionally, some direct methods to treat the hypersingularity have also been presented, such as semi-analytical integration with Cauchy Principal Value (CPV) (Guiggiani, Krishnasamy, Rudolphi and Rizzo, 1992), finite part concept (Hildenbrand, Kuhn, 1992), etc. In this paper, the indirect method of displacement-traction recovery method is adopted to treat the hypersingularity in the boundary. This method exploits the displacement gradients and traction relations, as well as the nodal displacements and tractions in the boundary, to establish the stress formulae for boundary nodes similar to the second equation in Eq.(32). But the kernel integrals are replaced by some algebraic and derivative expressions and accordingly no singularity appears.

3.4 Stress computation in elasto-plastic analysis

Eq.(33) consists of a number of nonlinear equations and some numerical techniques are necessary to treat these equations. The techniques to be introduced here are initial stress method and tangent predictor-radial return algorithm in the integration of the elasto-plastic constitutive equations. The initial stress method, which assumes the plastic stress as the initial stress, was described by Banerjee, Cathie and Davies (1979) in analyzing the isotropic elasto-plastic problems with the BEM, and the tangent predictor-radial return algorithm was first introduced by Nayak and Zienkiewicz (1972) in the FEM numerical analysis. This integration algorithm is widely used in numerical solution of stress with both the FEM and the BEM for its good accuracy. These two methods are implemented here through incremental iteration of the load.

For elasto-plastic analysis, if the load factor is $\Delta\alpha_i$ at every iterative step, the alternative incremental relations of stress in Eq.(33) is

$$\Delta\boldsymbol{\Sigma}^e = \Delta\alpha_i \mathbf{s} + \mathbf{T}_s \Delta\boldsymbol{\Sigma}^p \tag{40}$$

During the application of an increment of load, an element (or cell) or part of it may yield. All the stress quantities can be obtained with the elastic analysis by the BEM, and then the plastic state can be judged to occur or not at some points with reference to yield criterion. For any load increment, it is necessary to determine what proportion is elastic and what part is plastic with the elastic stress increment $\Delta\boldsymbol{\sigma}^e$, or trial stress increment. If the plastic deformation has occurred in current stress state ${}^t\boldsymbol{\sigma} + \Delta\boldsymbol{\sigma}^e$, when $f({}^t\boldsymbol{\sigma}) \le 0$ and $f({}^t\boldsymbol{\sigma} + \Delta\boldsymbol{\sigma}^e) > 0$, the portion of the stress increments that is greater than the yield stress value must be reduced to the yield surface, i.e. the following equation must hold true:

$$f({}^t\boldsymbol{\sigma} + m\Delta\boldsymbol{\sigma}^e) = 0 \tag{41}$$

and the reduction factor m can be solved with Eqs.(7) and (41) as:

$$m = \frac{-a_1 + \sqrt{a_1^2 - 4a_0 a_2}}{2a_2} \tag{42a}$$

where

$$\begin{cases} a_0 = ({}^t\boldsymbol{\sigma})^{\mathrm{T}} \mathbf{H} ({}^t\boldsymbol{\sigma}) - \overline{\sigma}_0^2 \\ a_1 = 2 (\Delta\boldsymbol{\sigma}^e)^{\mathrm{T}} \mathbf{H} ({}^t\boldsymbol{\sigma}) \\ a_2 = (\Delta\boldsymbol{\sigma}^e)^{\mathrm{T}} \mathbf{H} (\Delta\boldsymbol{\sigma}^e) \end{cases} \tag{43}$$

If the trial stress increment $\Delta\boldsymbol{\sigma}^e$ is sufficiently small compared to the stress ${}^t\boldsymbol{\sigma}$, the reduction factor m can also be obtained by this simple proportional relation:

$$m = \frac{\overline{\sigma}_0 - \overline{\sigma}_r}{\overline{\sigma}_{r+1} - \overline{\sigma}_r} \tag{42b}$$

where $\overline{\sigma}_r$ and $\overline{\sigma}_{r+1}$ are the equivalent stresses for previous and current stress states, respectively. Then with the help of Eq.(18), the stress increment $\Delta\boldsymbol{\sigma}$ can be calculated through the tangent predictor-radial return algorithm with the following equation (Fig. 3):

$$\Delta\boldsymbol{\sigma} = \Delta\boldsymbol{\sigma}^e - \frac{\mathbf{D}\mathbf{a}\mathbf{a}^{\mathrm{T}} (1-m) \Delta\boldsymbol{\sigma}^e}{\mathbf{a}^{\mathrm{T}}\mathbf{D}\mathbf{a}} \tag{44}$$

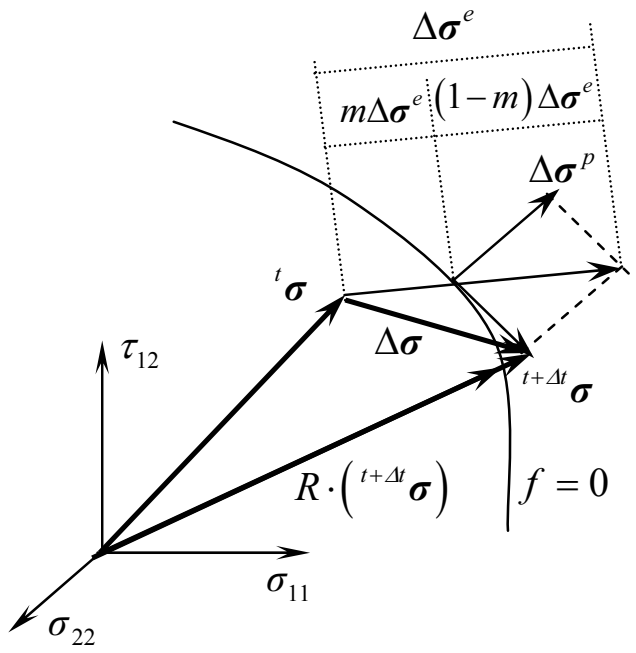

Figure 3 : Stress computation in the elasto-plastic analysis

and then the current stress can be renewed with:

$$ {}^{t+\Delta t}\boldsymbol{\sigma} = \left({}^{t}\boldsymbol{\sigma} + m\Delta\boldsymbol{\sigma}^e\right) + \Delta\boldsymbol{\sigma} \tag{45} $$

However, the stress obtained by Eq.(45) may depart a little from the yield surface usually, which can be practically eliminated by sufficiently small load increment. But the scaling factor R is also necessary to ensure that the final stress state lies on the yield surface, i.e. $\boldsymbol{\sigma} = R\cdot\left({}^{t+\Delta t}\boldsymbol{\sigma}\right)$ and $R = \overline{\sigma}_0/\overline{\sigma}_{r+1}$.

The above incremental iteration process with initial stress method can be summarized as follows:

- a) Assume an elastic behavior occurs and then the trial stress $\Delta\boldsymbol{\sigma}^e$ is obtained;
- b) Judge the elasto-plastic state and compute reduction factor m;
- c) Compute current stress increment $\Delta\boldsymbol{\sigma}$, and then renew current stress state ${}^{t+\Delta t}\boldsymbol{\sigma}$ and scale it to the yield surface;
- d) Continue with next Gauss point with starting from step a) until all Gauss points have been considered;
- e) Verify convergence with $\Delta\boldsymbol{\sigma}^p = \Delta\boldsymbol{\sigma}^e - \Delta\boldsymbol{\sigma}$ and accumulate the plastic stress, or initial stress, with ${}^{t+\Delta t}\boldsymbol{\sigma}^p = {}^{t}\boldsymbol{\sigma}^p + \Delta\boldsymbol{\sigma}^p$;
- f) Start next load increment with ${}^{t+\Delta t}\boldsymbol{\sigma}^p$ as the initial stress.

After the increment loops over, the final stress is solved and the accumulated plastic stress $\boldsymbol{\sigma}^p$ is obtained as well. The boundary values can be solved through the first equation in Eq.(33), and the internal displacements can also obtained by the third equation in Eq.(33) if necessary.

4 Numerical Examples

Two examples are presented here to demonstrate the application of the BEM to elasto-plastic analysis of 2-D orthotropic bodies by the proposed numerical scheme. The plane stress state is assumed and the elastic-perfectly plastic material model is adopted. In the numerical implementation, the 3-node quadratic element and 4-node quadrilateral linear element are used for the boundary elements and internal cells, respectively. The rectangular Cartesian coordinate directions are identical with the principal material directions.

Table 1 : Material properties of cantilever

Elastic constants		Strength properties	
E_1	74MPa	X	24MPa
E_2	85MPa	Y	230MPa
ν_{12}	0.26	S	48.9MPa
G_{12}	30MPa		

4.1 A cantilever under uniform load

In the first example, a homogenous orthotropic cantilever is considered, which is subjected to a transverse uniformly distributed load along one of the principal material direction (Fig. 4), and the material properties are listed in Table 1. The model is discretized with 377 nodes (including 80 boundary nodes), 40 boundary elements and 366 cells. The numerical solutions obtained by the present BEM are compared with the existing analytical results (Karakuzu and Ozcan, 1996), which were obtained on basis of the assumption that the stress component σ_y is equal to zero.

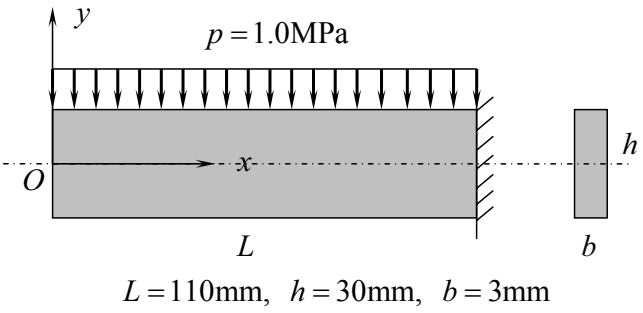

Figure 4 : A cantilever under uniform load

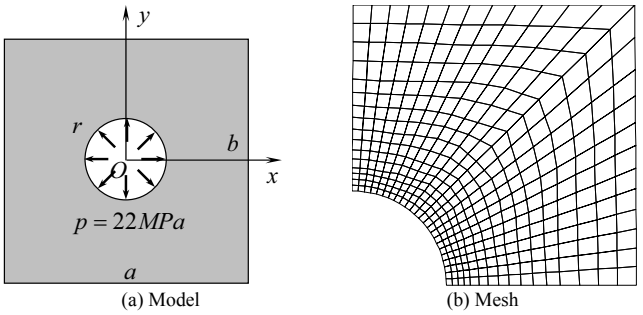

Figure 5 : A plate with hole under uniform internal pressure

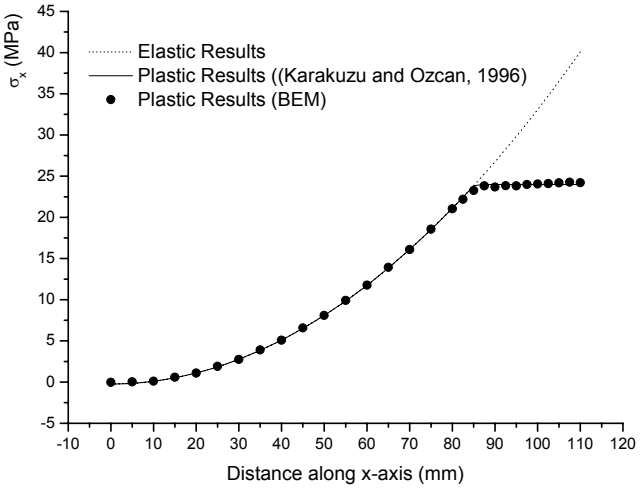

Figure 6 : Stress distribution along loaded side ($y = 15$mm)

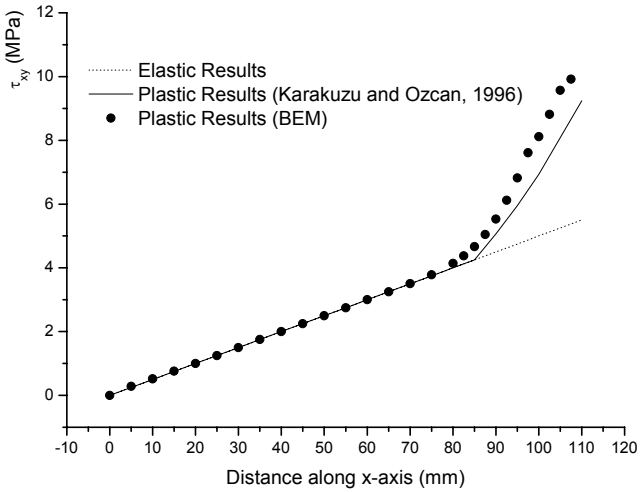

Figure 7 : Shear stress distribution along bent axis ($y = 0$mm)

The stress distributions along loaded side and bent axis are shown respectively in Fig. 6 and Fig. 7, where the elasto-plastic results are also compared with the elastic ones. These two figures show that plastic zone begins approximately at the section of $x = 85$mm. Fig. 8 $\sim$ Fig. 11 show the stress distributions along different x-sections. The results obtained by the BEM are generally in good agreement with the analytical ones. However, it should be pointed out that the analytical results (Karakuzu and Ozcan, 1996) are approximate on basis of the assumption that the stress component σ_y is equal to zero and the present numerical results are closer to the real solutions. It can be found from Fig. 10 and Fig. 11 that the plastic zone obtained by the BEM is slightly larger than that from the results (Karakuzu and Ozcan, 1996) near the fixed end.

The vertical displacements along the bent axis ($y = 0$mm) are shown in Fig. 12 and the elasto-plastic results are compared with the elastic ones.

4.2 A plate with hole under uniform pressure

This example is about a square orthotropic plate with hole under uniform internal pressure in the hole (Fig. 5a). The geometry is $a = b = 60$mm, $r = 10$mm and the magnitude of load is $p = 22$MPa. The material properties are listed in Table 2. Due to symmetry, a quarter of the plate is analyzed and the quarter-model is discretized with 425 nodes (including 80 boundary nodes), 40 boundary ele-

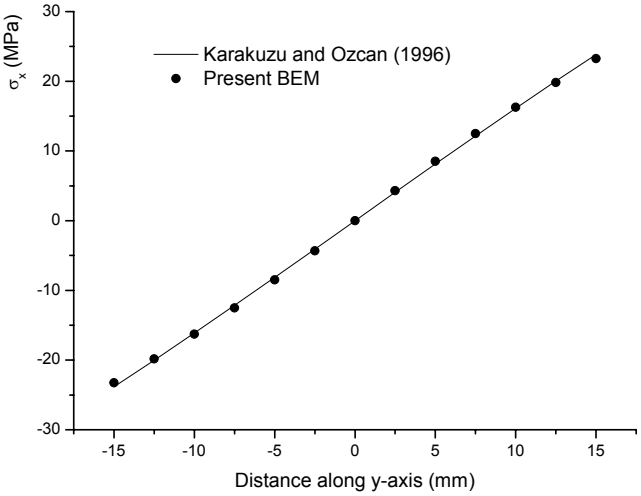

Figure 8 : Stress distribution along x-section ($x =$ 85mm)

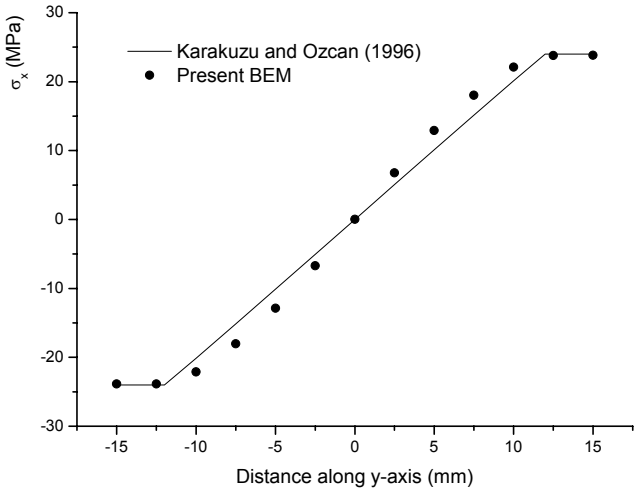

Figure 10 : Stress distribution along x-section ($x =$ 95mm)

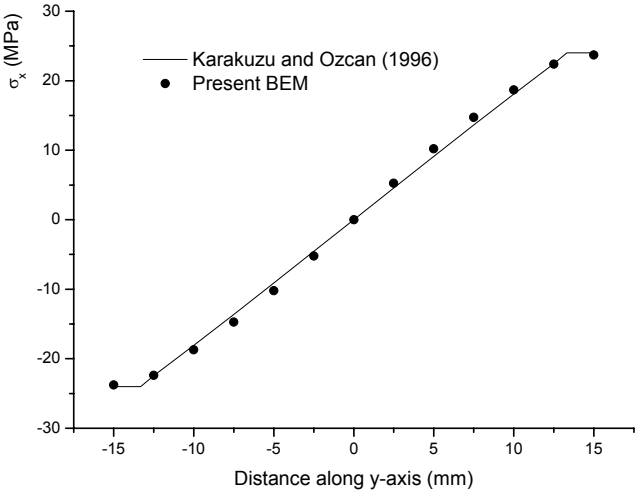

Figure 9 : Stress distribution along x-section ($x =$ 90mm)

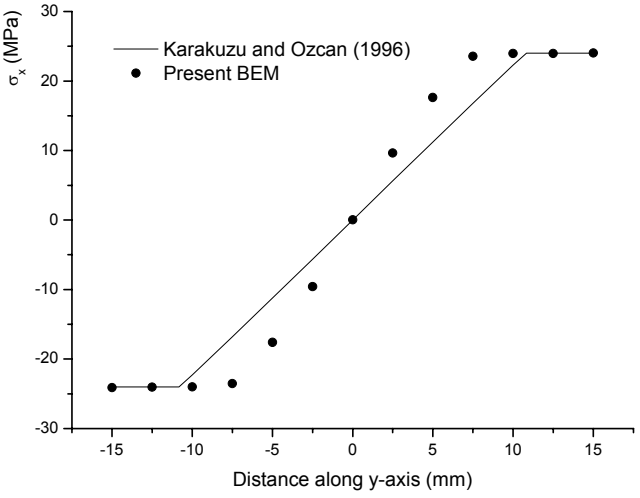

Figure 11 : Stress distribution along x-section ($x =$ 100mm)

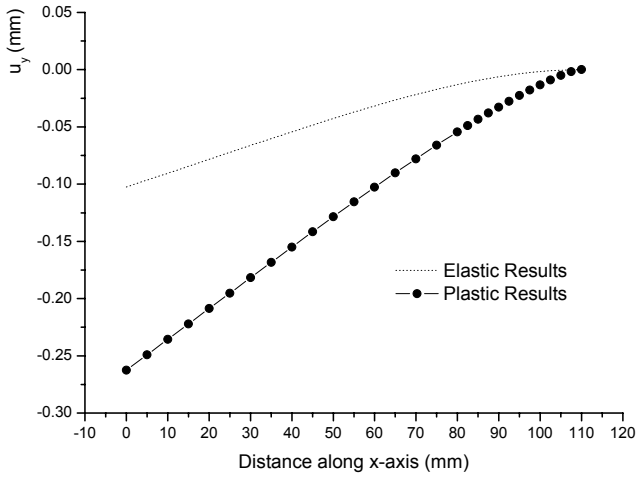

Figure 12 : Vertical displacements along the bent axis ($y = 0$mm)

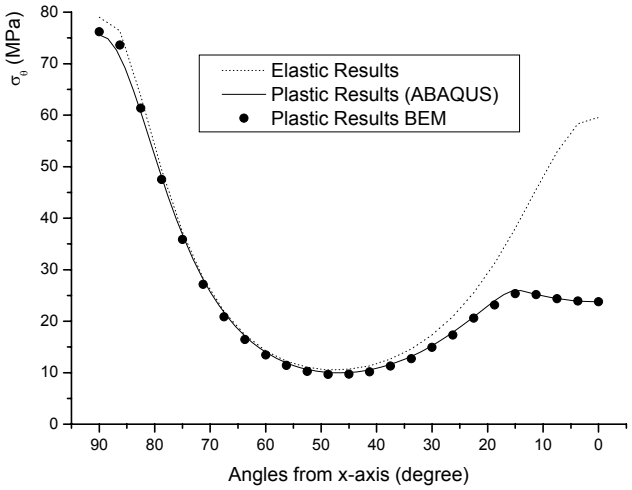

Figure 13 : Stress distribution along the circumference of the hole

Table 2 : Material properties of square-plate with hole

Elastic constants		Strength properties	
E_1	1.2GPa	X	230MPa
E_2	0.6GPa	Y	24MPa
ν_{12}	0.071	S	48.9MPa
G_{12}	0.07GPa		

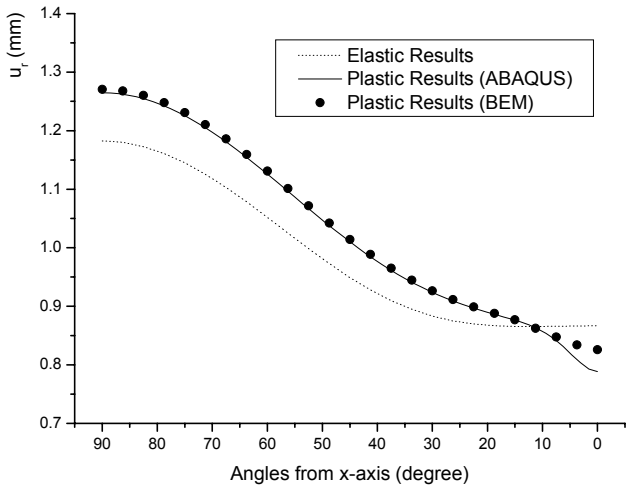

Figure 14 : Radial displacements of the hole

ments and 384 cells (Fig. 5b). The numerical solutions obtained by the BEM are compared with the results by commercial code ABAQUS.

For the FEM analysis with ABAQUS, 5200 CPS4R 4-node elements with 5361 nodes are used. The circumferential stress (σ_θ) and radial displacements (u_r) along the hole boundary are shown in Fig. 13 and Fig. 14, respectively, and the elastic results are plotted as well. It can be seen that the results obtained by the present BEM are in good agreement with those calculated by ABAQUS, except for slight differences of the displacements in several points near the x-axis, but the maximum error is less than 5%. The reason is that more exact displacement results can be obtained on the boundary with the BEM than with the FEM. Fig. 13 also shows that the area around the hole's boundary near x-axis is much easier to yield than that near y-axis.

Fig. 15 $\sim$ Fig. 18 plot the stress distributions in both elastic and elasto-plastic analyses along x-axis and y-axis, respectively. The present BEM results and the FEM results by ABAQUS are again in good agreement. Numerical results also show that there is a much greater elastic stress concentration near the hole in y-axis direction than that in x-axis direction as $E_1 > E_2$, but the plastic zone begins first around the x-axis near the hole, where the stress σ_y gives the major contribution to the yielding as $Y < X$. This means that the potential fracture would happen in the principal material direction with greater value of elastic modulus and strength property in the plate, which is quite different from that in the isotropic materials with isotropic yielding strength.

Fig. 19 and Fig. 20 show the deformation of the plate

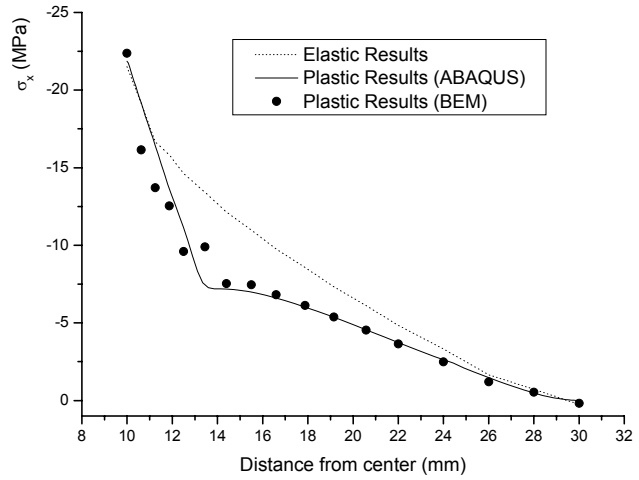

Figure 15 : Stress distribution along x-axis (σ_x)

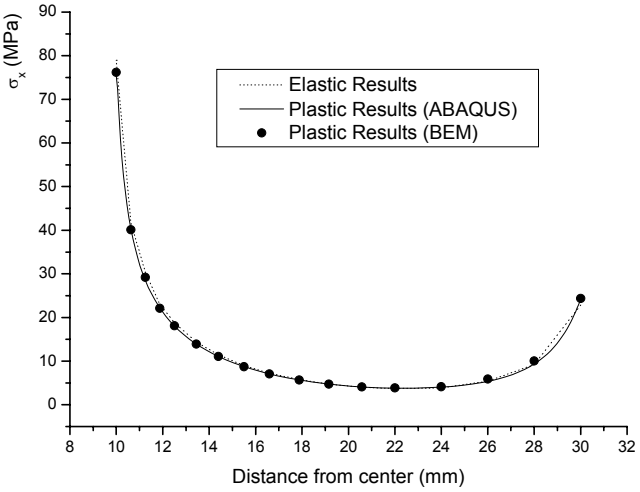

Figure 17 : Stress distribution along y-axis (σ_x)

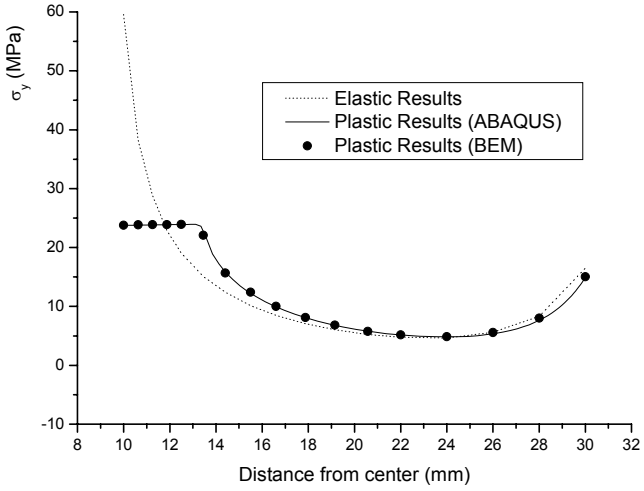

Figure 16 : Stress distribution along x-axis (σ_y)

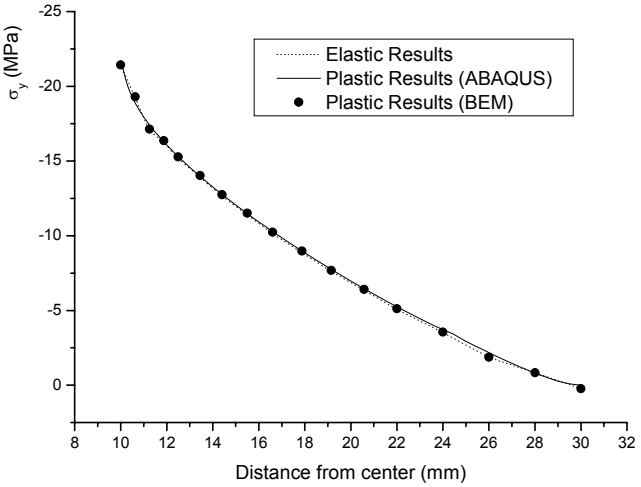

Figure 18 : Stress distribution along y-axis (σ_y)

along the x- and y-axis, respectively. It can be found that there is a greater deformation along the y-axis than that along the x-axis, which is resulted by different elastic moduli and strength properties in the two directions. The displacements u_x along x-axis (Fig. 19) with the BEM are little different from the results by ABAQUS, which is similar to the result in Fig. 14 and results from the fact that the boundary displacements obtained by the BEM are more exact than those by the FEM.

Fig. 21 shows the stress distributions along the direction of 45 degree from x-axis, i.e. diagonal direction in the plate. Fig. 22 contours the equivalent stress distributions throughout the plate, which clearly shows the plastic zones and the elasto-plastic stress distributions in the plate.

5 Conclusions

In this paper, a numerical scheme for elasto-plastic analysis of 2-D orthotropic problems with the BEM is developed. The discretized equations and iterative equations for numerical implementation are presented based on the boundary integral equations, internal values and fundamental solutions for orthotropic bodies. Numerical integral techniques, including coordinate transformations, rigid displacement solution or constant plastic so-

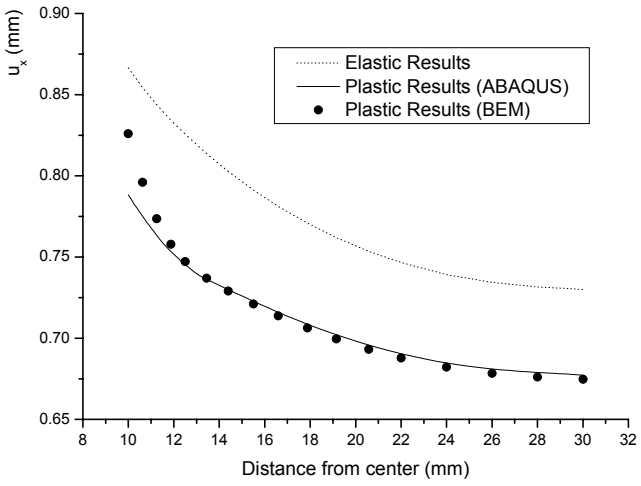

Figure 19 : Displacements in x-axis (u_x)

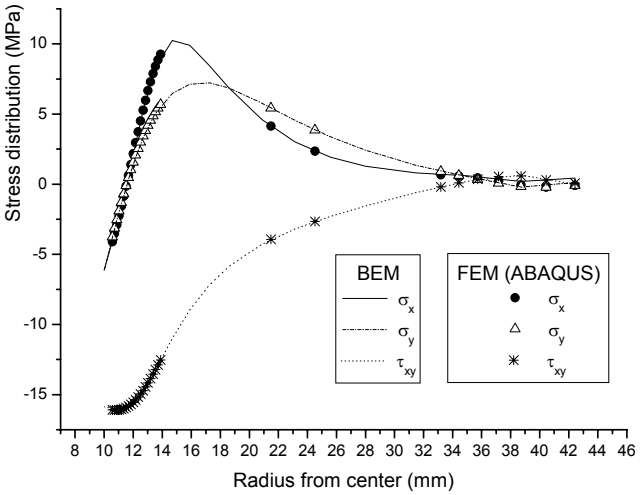

Figure 21 : Stress distribution along the direction of angle 45 degree from x-axis

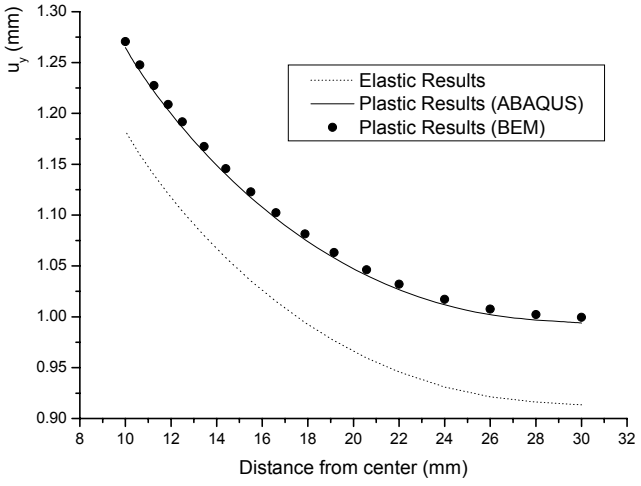

Figure 20 : Displacements in y-axis (u_y)

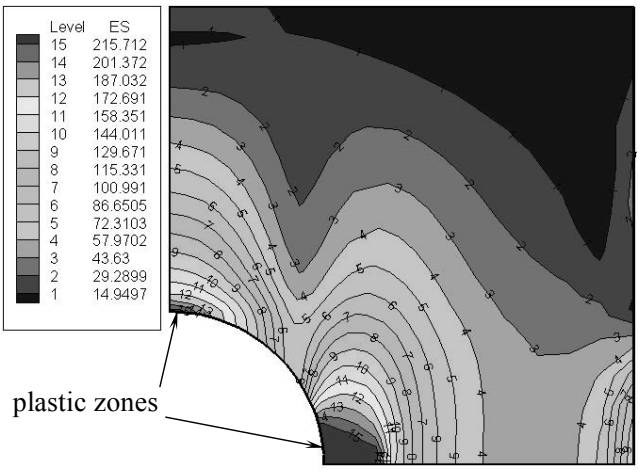

Figure 22 : The equivalent stress contour in the plate

lution, and displacement-traction recovery method, are introduced to remove all kinds of singularities in the integral equations. The Hill orthotropic yield criterion is adopted in the plastic analysis. The initial stress method and tangent predictor-radial return algorithm are used to compute the stress in the elasto-plastic analysis with incremental iteration scheme. Numerical examples show that the results obtained by the present BEM are in good agreement with the existing ones or those obtained by the FEM. The computational results demonstrate the validity and reliability of the developed numerical scheme.

Acknowledgement: This project was supported by the Basic Research Foundation of Tsinghua University, the National Foundation for Excellent Doctoral Thesis (200025) and the National Natural Science Foundation of China (19902007).

References

Aliabadi, M. H. (2002): The Boundary Element Method – Volume 2: Applications in Solids and Structures, John Wiley & Sons, Chichester.

Atluri, S. N.; Han, Z. D.; Shen, S. (2003): Meshless local Petrov-Galerkin (MLPG) approaches for solving the weakly-singular traction & displacement boundary integral equations. *CMES: Computer Modeling in Engineering & Sciences*, vol. 4, No. 5, pp. 507-517.

Banerjee, P. K.; Cathie, D. N.; Davies, T. G. (1979): Two and three dimensional problems of elasto-plasticity. In: P. K. Banerjee; R. Butterfield (eds) *Developments in Boundary Element Methods-1*. Elsevier, London, pp. 65-95.

Banerjee, P. K.; Henry, D. P.; Raveendra, S. T. (1989): Advanced inelastic analysis of solids by the boundary element method. *International Journal of Mechanical Sciences*, vol. 31, pp. 309-322.

Bonnet, M.; Mukherjee, S. (1996): Implicit BEM formulations for usual and sensitivity problems in elasto-plasticity using the consistent tangent operator concept. *International Journal of Solids and Structures*, vol. 33, pp. 4461-4480.

Brebbia, C. A.; Telles, J. C. F.; Wrobel, L. C. (1984): Boundary Element Techniques: Theory and Applications in Engineering, Springer-Verlag, New York.

Bui, H. D. (1978): Some remarks about the formulation of three-dimensional thermoelastoplastic problems by integral equations. *International Journal of Solids and Structures*, vol. 14, No. 11, pp. 935-939.

Carrer, J. A. M.; Telles, J. C. F. (1992): A boundary element formulation to solve transient dynamic elasto-plastic problems. *Computers and Structures*, vol. 45, pp. 707-713.

Cen, Z. Z. (1984): Three-dimensional Elasto-plastic Analysis with Coupling Method of the FEM and the BEM, Ph.D. dissertation, Department of Engineering Mechanics, Tsinghua University.

Chopra, M. B.; Dargush, G. F. (1994): Development of BEM for thermoplasticity. *International Journal of Solids and Structures*, vol. 31, pp. 1635-1656.

Dong, C. Y. (1992): Some Basic Aspects on the Boundary Element Methods in Elastoplasticity and Their Applications on Contact Problems, Ph.D. dissertation, Department of Engineering Mechanics, Tsinghua University.

Dong, C. Y.; Lo, S .H.; Cheung, Y. K. (2002): Application of the boundary-domain integral equation in elastic inclusion problems. *Engineering Analysis with Boundary Elements*, vol. 26, No. 6, pp. 471-477.

Du, Q. H.; Cen, Z. Z.; et al. (1989): The Boundary Integral Equation Method – Boundary Element Method, Higher Education Press, Beijing

Green, E. (1943): A note on stress systems in aeolotropic materials. *Philosophical Magazine*, vol. 34, pp. 416-418.

Guiggiani, M.; Krishnasamy, G.; Rudolphi, T. J.; Rizzo, F. J. (1992): A general algorithm for the numerical solution of hypersigular boundary integral equations. *ASME Journal of Applied Mechanics*, vol. 59, pp. 604-614.

Han, Z. D.; Atluri, S. N. (2003): On some formulations of weak-singular traction & displacement BIE, and their solutions through Petrov-Galerkin approaches. *CMES: Computer Modeling in Engineering & Sciences*, vol. 4, No. 1, pp. 5-20.

Henry, D. P.; Banerjee, P. K. (1988): A new BEM formulation for two- and three-dimensional elastoplasticity using particular integrals. *International Journal for Numerical Methods in Engineering*, vol. 26, pp. 2079-2096.

Hildenbrand, J.; Kuhn, G. (1992): Numerical computation of hypersingular integrals and application to the boundary integral equation for stress tensor. *Engineering Analysis with Boundary Elements*, vol. 10, pp. 209-217.

Hill R. (1948): A theory of the yielding and plastic flow of anisotropic metals. *Proceedings of the Royal Society of London*, vol. A193, pp. 281-288.

Hill, R. (1983): The Mathematical Theory of Plasticity, Oxford University Press, Oxford.

Huang, L. X.; Sun, X. S.; Liu, Y. H.; Cen, Z. Z. (2004): Parameter identification for two-dimensional orthotropic material bodies by the boundary element method. *Engineering Analysis with Boundary Elements*, vol. 28, No. 2, pp. 109-121.

Karakuzu, R.; Ozcan, R. (1996): Exact solution of elasto-plastic stresses in a metal-matrix composite beam of arbitrary orientation subjected to transverse loads. *Computers Science and Technology*, vol. 56, pp. 1383-1389.

Karakuzu, R.; Sayman, O. (1994): Elasto-plastic finite element analysis of orthotropic rotating discs with holes. *Computers and Structures*, vol. 51, No. 6, pp. 695-703.

Kumar, V.; Mukherjee, S. (1977): A boundary integral equation formulation for time dependent inelastic deformation in metals. *International Journal of Mechanical Sciences*, vol. 19, No. 12, pp. 713-724.

Lekhnitskii, S. G. (1968): Anisotropic Plates, Gordon and Breach, New York.

Mendelson A. (1973): Boundary integral methods in elasticity and plasticity. *NASA TN-D-7418*.

Mukherjee, S. (1977): Corrected boundary integral equations in planar thermoelastoplasticity. *International Journal of Solids and Structures*, vol. 13, No. 4, pp. 331-336.

Nayak, G. C.; Zienkiewicz, O. C. (1972): Elasto-plastic stress analysis: a generalization for various constitutive relations including strain softening. *International Journal for Numerical Methods in Engineering*, vol. 15, pp. 113-135.

Ochiai, Y.; Kobayashi, T. (1999): Initial stress formulation for elastoplastic analysis by improved multiple-reciprocity boundary element method. *Engineering Analysis with Boundary Elements*, vol. 23, pp. 167-173.

Okada, H.; Atluri, S. N. (1994): Recent developments in the field-boundary element method for finite/small strain elastoplasticity, *International Journal of Solids and Structures*, vol. 31, pp. 1737–1775.

Okada, H.; Rajiyah, H.; Atluri, S. N. (1989): Non-hyper-singular integral representations for velocity (displacement) gradients in elastic/plastic solids (small or finite deformations). *Computational Mechanics*, vol. 4, pp. 165-175.

Owen, D. R. J.; Figuerias, J. A. (1983): Anisotropic elasto-plastic finite element analysis of thick and thin plates and sheets. *International Journal for Numerical Methods in Engineering*, vol. 19, pp. 541-566.

Partridge, P. W.; Brebbia, C. A.; Wrobel, L. C. (1992): The Dual Reciprocity Boundary Element Method, Computational Mechanics Publications, Southampton.

Rizzo, F. J.; Shippy, D. J. (1970): A method for stress determination in plane anisotropic elastic bodies. *Journal of Composite Materials*, vol. 4, No. 1, pp. 36-61.

Sladek, J.; Sladek, V. (1995): Boundary element method for thermoelastoplastic problems. *International Journal for Numerical Methods in Engineering*, vol. 38, pp. 3635-3652.

Sun, X. S.; Cen, Z. Z. (2002): Further improvement on fundamental solutions of plane problems for orthotropic materials. *Acta Mechanica Solida Sinica*, vol. 15, No. 2, pp. 171-181.

Swedlow, J. L.; Cruse, T. A. (1971): Formulation of boundary integral equation for three-dimensional elasto-plastic body. *International Journal of Solids and Structures*, vol. 7, No. 12, pp. 1673-1683.

Tan, C. L.; Gao, Y. L. (1992): Boundary element analysis of plane anisotropic bodies with stress concentrations and cracks. *Composite Structures*, vol. 20, pp. 17-28.

Telles, J. C. F.; Brebbia, C. A. (1979): On the application of the boundary element method to plasticity. *Applied Mathematical Modelling*, vol. 3, pp. 466-470.

Vaziri, R.; Olson, M. D.; Anderson, D. L. (1992): Finite element analysis of fibrous composite structures: a plasticity approach. *Computers and Structures*, vol. 44, No. 1-5, pp. 103-116.

Zhang, C. (2002): A 2-D time-domain BIEM for dynamic analysis of cracked orthotropic solids. *CMES: Computer Modeling in Engineering & Sciences*, vol. 3, No. 3, pp. 381-398.